

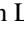

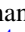
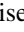


Spontaneous polarization and pyroelectric coefficient of lithium niobate and lithium tantalate determined from crystal structure data

Tina Weigel ^{1,2,*}, Christian Ludt ², Tilmann Leisegang ², Erik Mehner,² Sven Jachalke ³, Hartmut Stöcker ²,
Thomas Doert ⁴, Dirk C. Meyer,^{1,2} and Matthias Zschornak^{1,2}

¹Center for Efficient High Temperature Processes and Materials Conversion ZeHS, TU Bergakademie Freiberg,
Winklerstr. 5, 09599 Freiberg, Germany

²Institute of Experimental Physics, Technische Universität Bergakademie Freiberg, Leipziger Str. 23, 09599 Freiberg, Germany

³NaMLab gGmbH, Nöthnitzer Str. 64a, 01187 Dresden, Germany

⁴Faculty of Chemistry and Food Chemistry, Technische Universität Dresden, 01062 Dresden, Germany



(Received 16 June 2023; accepted 21 July 2023; published 17 August 2023)

This work shows an alternative approach to extract the pyroelectric coefficient directly from the response of the crystal structure to temperature variations. The approach uses crystal structure parameters determined at different temperatures and Born effective charges calculated by density functional theory to evaluate the spontaneous polarization. On this basis, the pyroelectric coefficient is calculated using the first derivative of the polarization with respect to temperature. In this work, we utilize laboratory single-crystal x-ray diffraction in a temperature range from 80 to 400 K to demonstrate this approach on the standard pyroelectric materials lithium niobate and lithium tantalate. The accuracy of the presented method for the spontaneous polarization is on par with reported experimental data and relative errors are below 7%. Our determined pyroelectric coefficients have larger errors, but are within the range of reported literature values. The outlined semitheoretical method is recommended when electrical characterization under temperature change is not feasible, e.g., when the preparation of large area contacts is problematic or only small sample volumes are available ($<100 \mu\text{m}^3$).

DOI: [10.1103/PhysRevB.108.054105](https://doi.org/10.1103/PhysRevB.108.054105)

I. INTRODUCTION

Pyroelectric materials respond to a change in temperature with a change in spontaneous polarization \vec{P}_S . These materials are important for many key applications [1] in the technological fields of sensing and detection [2–6], x-ray sources [7], water disinfection [8,9], hydrogen generation [10–13], as well as energy conversion and recovery [1,14–18]. For a characterization of pyroelectric materials, the reliable assessment of pyroelectric properties is necessary. The pyroelectric coefficient $\vec{p} = \frac{d\vec{P}_S}{dT}$, i.e., the temperature derivative of the spontaneous polarization, is an experimentally accessible quantity and various static and dynamic measurement methods exist [19,20]. The spontaneous polarization \vec{P}_S can be experimentally determined with electric measurements [21–25] as well, but a theoretical estimation of both parameters is difficult. The required computing of temperature-dependent properties is not straightforward, computationally expensive, and limited to simple structures [26–30]. Furthermore, the calculations have uncertainties due to the used approximations and inaccurate interatomic potentials [28–30]. An alternative procedure to access pyroelectric properties is important, specifically where electric measurements are difficult or even not feasible, e.g., if large area contacts are not possible, the sample is conductive, or the

pyroelectric signal is overlaid with other disturbing effects, e.g., thermally stimulated currents [19].

Finding an adequate theory, which correctly describes the polarization in a material is a challenge [31]. A standard approach to quantify the polarization is the model of Clausius [32] and Mossotti [33] (CM model), which defines \vec{P}_S as the sum of the dipoles within the unit-cell volume. Hereby, the polarization represents an absolute value and the presence of individual polar units in the structure is assumed. Unfortunately, this is not a realistic picture [31]. A better definition of polarization emerged in the early 1990s, referred to as “modern theory of polarization” (MTP) by Resta [34], King-Smith *et al.* [35], and Vanderbilt *et al.* [36], describing the polarization as a difference polarization between two distinct states. Following this approach, \vec{P}_S can be calculated using first-principle methods [26,37–45]. For example, Peng and Cohen [26] used the MTP to calculate \vec{P}_S with first-principle computed structural parameters and Born effective charges (BEC). They recommended to use experimental crystal structure data in order to improve this approach for determining \vec{P}_S as they seem more reliable. Furthermore, calculation of various other physical properties depending on \vec{P}_S was successful and good comparability with theoretical data was reached [26], however, with larger deviation to experimental data [46].

This work demonstrates the determination of \vec{P}_S and \vec{p} from experimental single-crystal x-ray diffraction (SC-XRD) data and BEC computed by density functional theory (DFT) using the MTP. For this purpose, the well-known and thoroughly investigated [47–55] pyroelectric standard materials

*tina.weigel@physik.tu-freiberg.de

lithium niobate (LiNbO_3) and lithium tantalate (LiTaO_3) were chosen. We compare \vec{P}_S and \vec{p} from SC-XRD structural data (semithoretical approach) with DFT-calculated values based on structural data from SC-XRD and directly from DFT (theoretical approach), with measured \vec{p} values obtained by means of the Sharp-Garn method [56,57], as well as with theoretical and experimental values from literature. Following the semithoretical method, the pyroelectric coefficient of a crystal can be directly estimated from the structural characterization by x-ray diffraction with no additional measurements or knowledge of other material parameters, which should be of interest for optimization and analysis of known and novel pyroelectrics. The presented approach can be used for all characterization methods that provide access to temperature-dependent structural parameters.

II. METHODOLOGY

A. Single-crystal x-ray diffraction

In this work, congruent (nonstoichiometric) LiNbO_3 (C-LN) from CrysTec GmbH, Berlin, Germany, and stoichiometric LiNbO_3 (S-LN) from SurfaceNet GmbH, Rheine, Germany, and congruent LiTaO_3 (C-LT) crystals from Epcos AG, Munich, Germany, are used. The stoichiometric material is in fact near-stoichiometric with a $[\text{Li}]/[\text{Nb}]$ atomic ratio of 49.7/50.3 for S-LN and will be treated as stoichiometric for simplicity in the following. Well-defined single crystals with a size of around $(50 \times 50 \times 50) \mu\text{m}^3$ were prepared with a focused ion beam technique [58], that especially allows the accurate absorption correction. Thus, a small SC-XRD sample is cut from a bigger crystal plate, which remains usable for additional measurements, here the pyroelectric characterization by conventional methods. The x-ray diffraction experiment was performed with a Bruker D8 Quest [59] single-crystal x-ray diffractometer on these samples in a temperature range from 80 to 400 K. The temperature was adjusted with a liquid nitrogen stream generated by a Kryoflex II low-temperature system. For the experiment, $\text{Mo-K}\alpha$ radiation ($\lambda = 0.71076 \text{ \AA}$) was used. With a frame width of 0.5° and an exposure time of 45 s (LiNbO_3) and 55 s (LiTaO_3), respectively, a reciprocal space sphere of $2\theta \leq 117.1^\circ$ with a resolution of $\sin \theta_{\text{max}}/\lambda = 1.2 \text{ \AA}^{-1}$ was measured. Data integration, reduction, and absorption correction with a numerical approach were done with the APEX3 [60] software. The software JANA2006 [61] was used for extinction correction (type I, Lorentz mosaic distribution), structure determination, and structure parameter refinement. Details of the measurement conditions, data reduction, and refinement can be found elsewhere [58]. All errors of crystal structure parameters are given at the 1σ level.

B. Density functional theory

The calculations of the electron density and structure of LiNbO_3 and LiTaO_3 were performed with the *ab initio* simulation software VASP [62] and the projector-augmented wave method (PAW) [63]. Generalized gradient approximation (GGA) was chosen in PBE parametrization [64] to account for the exchange-correlation functional. The total energies converged within 10^{-7} eV with a maximum kinetic

energy of 450 eV for the basis of plane waves and the Γ point centered in a $12 \times 12 \times 4$ k -point mesh according to Monkhorst and Pack [65]. The sampling of this mesh is finer than $0.02 \times 2\pi \text{ \AA}^{-1}$. Atom positions and cell parameters were completely relaxed in the chosen space group with residual forces less than $10^{-4} \text{ eV \AA}^{-1}$.

To account for the nonzero temperature, the experimentally determined lattice parameters were used for atomic relaxation of the internal degrees of freedom for each ion. The 0-K value is approximated by extrapolation with the respective linear thermal expansion parameter (see Appendix A). Additionally, the system was also fully relaxed regarding the inner degrees of freedom plus the lattice parameters (ground state, GS).

Subsequently, BEC were computed by means of density functional perturbation theory on the basis of DFT-relaxed structures, as implemented in the VASP code. The convergence criterion was changed to 10^{-9} eV to obtain highly precise BEC. The BEC tensors were calculated for GS and for the relaxed structures at nonzero temperature. Additionally, the macroscopic electric polarization was determined by the evaluation of Berry phase expressions (to obtain the polarization directly from DFT calculations) according to the MTP [34–36], for comparison. For the normalization of the absolute polarizations, the paraelectric phases of LiNbO_3 and LiTaO_3 were computed with DFT as well.

C. Sharp-Garn method

The pyroelectric coefficients of C-LN, S-LN, and C-LT were measured with the Sharp-Garn-method [56,57]. Hereby, the sample is stimulated with a sinusoidal temperature signal while measuring the generated electric current. The phase shift between both signals allows to cleanly separate the thermally induced current (from trapped charges) and the actual pyroelectric contribution.

For the measurements, large single-crystal plates ($5 \times 5 \times 0.2 \text{ mm}^3$) of LiNbO_3 and LiTaO_3 were contacted with silver electrodes [66]. The same crystal plates were used for the SC-XRD sample preparation. The pyroelectric coefficient was measured in an evacuated chamber, where the samples were contacted with a metallic needle as top contact [20,67]. Measurements were carried out in a temperature range from 273 to 400 K, with a sinusoidal temperature stimulation having an amplitude of $\pm 2 \text{ K}$, a frequency of $f = 0.0005 \text{ Hz}$, and an average heat-up rate of 5 Kh^{-1} .

D. Calculation of the spontaneous polarization and the pyroelectric coefficient from crystal structure parameters

The materials LiNbO_3 and LiTaO_3 belong to the crystal class $3m$ [68], so that the pyroelectric coefficient is composed of $\vec{p} = p_3 \cdot \vec{e}_3$ [69], with \vec{e}_3 being parallel to the lattice vector \vec{c} . Contributions in \vec{e}_1 and \vec{e}_2 directions compensate to zero and the pyroelectric coefficient can be described by the scalar p . Consequently, \vec{P}_S has contributions in c direction only and will also be given as a scalar P_S .

According to the MTP, P_S can be calculated using the BEC tensor $Z_{j,kl}^*$ and the atomic displacements $u_{j,l}$ for every atom j of the structure with regard to a phase transition from a polar

to a nonpolar phase:

$$P_{S,k} = \frac{e}{V_{UC}} \sum_{j=1}^N Z_{j,kl}^* u_{j,l}, \quad (1)$$

where k and l label Cartesian directions, e is the elementary charge, V_{UC} is the unit-cell volume, and N is the number of atoms in the unit-cell. The atomic displacements $u_{j,l}$ are the difference of the experimentally determined atomic positions of the ferroelectric phase and the atomic positions of the paraelectric phase. According to Inbar and Cohen [70,71] the origin of pyroelectricity in LiNbO_3 and LiTaO_3 is a coupled movement of lithium and oxygen atoms in opposite directions parallel to the c axis.

The pyroelectric coefficient p results from the slope of P_S between two temperature points and is calculated from the first derivative (under constant electric field E and elastic strain σ) [72]:

$$p = \left(\frac{dP_S}{dT} \right)_{E,\sigma}. \quad (2)$$

This is the so-called primary pyroelectric effect. Besides, additional effects contribute to the pyroelectric behavior of a material [19]:

$$p_k = \underbrace{\frac{\partial P_{S,k}}{\partial T}}_{p_{\text{prim}}} + \underbrace{\sum_{l,m} \frac{\partial (d_{klm} \sigma_{lm})}{\partial T}}_{p_{\text{sec}}} + \underbrace{\sum_{l,m,n} \frac{\partial (\mu_{klmn} \frac{\partial e_{lm}}{\partial T_n})}{\partial T}}_{p_{\text{ter}}} + \dots \quad (3)$$

Hereby, materials with piezoelectric properties (piezoelectric tensor d_{klm}) respond to thermally induced mechanical strain according to the stress tensor σ_{lm} , which generates charges. This is called secondary pyroelectric effect. The tertiary pyroelectric and other effects are described in Refs. [19,20,72] and are not considered in the following.

III. RESULTS

A. Thermal expansion

We compare the temperature dependence of the lattice parameters a and b , the unit-cell volume V_{UC} , and the free coordinates of lithium z_{Li} , transition metal $z_{\text{Nb/Ta}}$, and oxygen z_{O} for experimental SC-XRD structural parameters [73] and DFT-relaxed atomic positions (see Fig. 1). The SC-XRD determined lattice parameters show discrepancies, which within their individual errors do not join into a smooth continuous temperature dependence. This can be explained since modern integration programs for SC-XRD data underestimate the errors of the lattice parameters due to the least-square refinement. In a work by Guzei *et al.* [74], it is shown that the standard deviation of a reference sample, measured in different experiments, is approximately 23 times higher than for the individual experiment. To eliminate experimental deviations in the progression of thermal expansion, the structural data from SC-XRD, which are also used to model the temperature-dependent lattice for DFT, were fitted. Quadratic degrees of freedom were chosen (solid lines in Fig. 1) according to Kim *et al.* [75]. The higher-order T^3 dependence, to describe real crystal lattices at temperatures below $T = \frac{\theta_D}{50}$ (with θ_D the Debye temperature) [76], was neglected, as an influence would

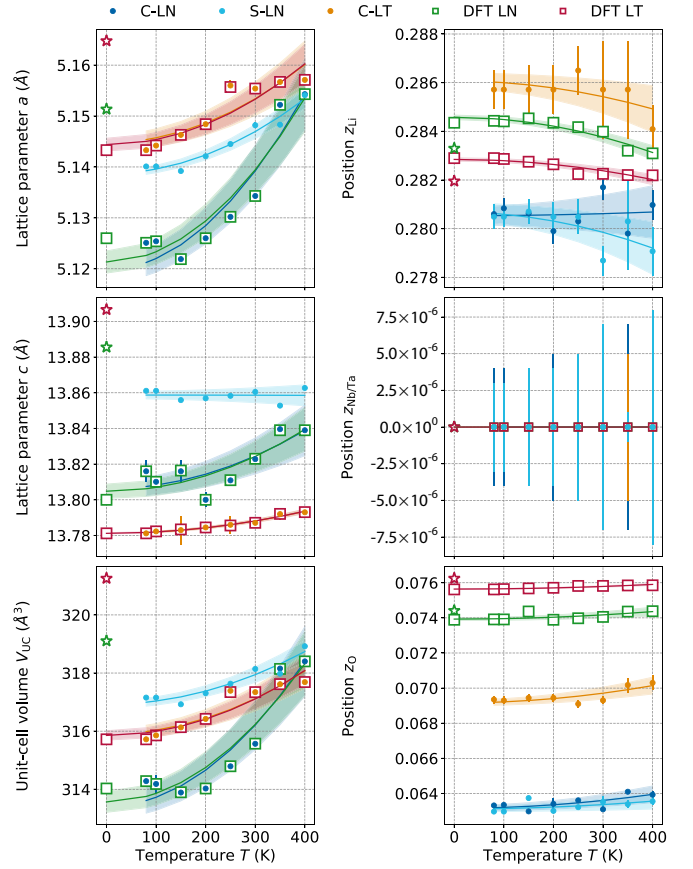


FIG. 1. Temperature-dependent lattice parameters $a(T)$ and $c(T)$, unit-cell volume $V_{UC}(T)$, as well as coordinates $z_{\text{Li}}(T)$, $z_{\text{Nb/Ta}}(T)$, and $z_{\text{O}}(T)$, for experimentally determined (\bullet) structures of C-LN (blue), S-LN (cyan), C-LT (orange), and DFT-calculated structures of LN (green) and LT (red). DFT-calculated structures were relaxed with experimental temperature dependencies and the extrapolated 0-K unit cells (\square) as constraints. Additionally, fully relaxed theoretical structures in GS (\star) are given as well. The SC-XRD structural parameters and DFT-computed data using the same structural parameters were smoothed with respect to the progression of thermal expansion by a quadratic fit (solid lines). The light colored areas indicated the 1σ confidence intervals of the fit.

be excepted only at $T \leq 10$ K [77]. The following calculations are based on the fitted structural parameters, free of errors from data reduction.

The comparison of the 0-K lattice parameters, estimated from the expansion coefficient and experimental lattice parameters, with the full theoretical DFT-GS lattice parameters also show a discrepancy. The reason is that the GGA in PBE parametrization generally overestimates lattice parameters in solids [78] for the GS. In this study, the GS lattice parameter a is 0.5% larger for both materials and c is 0.7% larger for LiNbO_3 and 1.0% larger for LiTaO_3 compared to the experimental values.

When comparing both experimentally and theoretically determined atomic displacements upon temperature increase, especially for the oxygen displacements, it is evident that the positional changes found by DFT in general do not reach the extent of the experimental values, even though the constrained

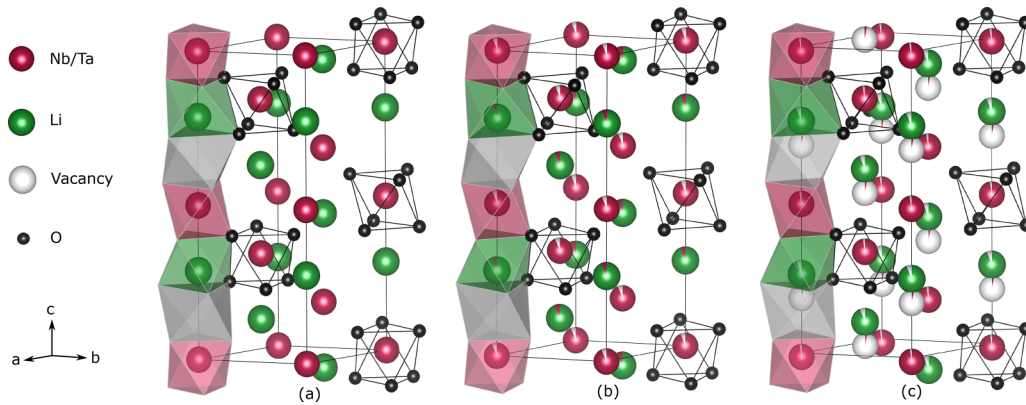


FIG. 2. Structure models for the SC-XRD refinement: (a) stoichiometric, (b) defect model for congruent LiNbO_3 with Li (green) deficiency and Li as well as Nb (red) on the Li site, and (c) defect model for congruent LiTaO_3 with Li deficiency and Ta (red) on the Ta site and within the vacant (gray) octahedron. For simplification, we do not show all O ions and oxygen bonds (black). Figures were produced using VESTA3 [82].

cell dimensions have been set to the experimental parameters. This can be expected since the theory does not describe thermal ionic motion and underestimates the displacement from the center of charge. Since oxygen carries about two to three times the charge of lithium, this underestimation introduces a significant deviation in the theoretical spontaneous polarization.

B. Calculation of spontaneous polarization

Since congruent LiNbO_3 and LiTaO_3 samples were also measured, the additional influence of defect polarization needs to be taken into account. The structure models we used for our SC-XRD refinement are based on the predominant atomistic models as discussed in literature [79–81] consistent with the diffraction data and visualized in Fig. 2. We refined the defect structure of LiNbO_3 according to the results of Zotov *et al.* [79] and Abrahams *et al.* [80] [see Fig. 2(b)], with a Li deficiency and Nb occupying the Li site. We obtained an Li site occupancy of 0.944(2) and a Nb occupancy of 0.056(10) on the Li site, which are comparable with the results of Abrahams *et al.* [80]. A $[\text{Li}]/[\text{Nb}]$ atomic ratio of 48.9(2)/51.1(2) follows from the refined defect structure, which is in agreement with the literature value of $[\text{Li}]/[\text{Nb}] = 48.5/51.5$ [83,84]. For LiTaO_3 we used the defect model of Vyalikh *et al.* [81] [see Fig. 2(c)] with a Li deficiency and Ta occupying the vacant O octahedron. We obtained an occupancy of 0.935(10) for Li, 0.9705(8) for Ta on the Ta site, and 0.029(10) for Ta in the nominally vacant octahedron. This corresponds to a $[\text{Li}]/[\text{Ta}]$ atomic ratio of 48.7(2)/51.3(2), i.e., it is the same value as Vyalikh *et al.* [81] and Köhler *et al.* [85] determined for crystals from the same manufacturer and it is in perfect agreement with the literature value of $[\text{Li}]/[\text{Ta}] = 48.75/51.25$ [86] as well. Because we measured the same crystals for all temperatures, we assumed the refined occupancy model of $T = 300$ K to be valid for all measurements. This is reasonable because changes of the defect structure [87] and LiO_2 self-diffusion can only be observed above 425 K [88]. Low temperatures affect only the degree of defect disorder [89]. It has to be noted that the refinement of occupancy factors is difficult for LiNbO_3 and LiTaO_3 due to the

low scattering factors of Li compared to the large scattering factors of Nb and Ta [90].

To apply Eq. (1), we determined the atomic displacements $u_{j,l}$ using the structure solutions of the paraelectric phase of Boysen *et al.* [91] for LiNbO_3 and of Abrahams *et al.* [92] for LiTaO_3 to acquire the SC-XRD-based values. For the DFT-based values we used the relaxed structure of the computed paraelectric phase to calculate $u_{j,l}$. Furthermore, we used the fitted crystal structure parameters from Fig. 1 of the ferroelectric phase for the calculations.

To evaluate the influence of BEC changes with temperature on the spontaneous polarization P_S and with the aim to keep computational cost for the semitheoretical method minimal, we tested the routines using BEC tensors computed at every temperature step (Model 1) as well as exclusively the BEC tensors of the GS for all temperatures (Model 2). The results are shown in Fig. 3 for the SC-XRD data of C-LN and C-LT. An explicit development of BEC components with temperature is given in Appendix B. Since BEC tensors vary less than 1% (in average) within the considered temperature range, both curves are equivalent for LiTaO_3 (discrepancies below 0.2%). The variations of the BEC tensors are up to 3% for LiNbO_3 , which are visible in the discrepancy (up to 0.5%) between Models 1 and 2 in Fig. 3(a). A second SC-XRD data set for LiNbO_3 (dashed-dotted line in Fig. 3) reproduces the results from the first measurement with good precision, i.e., a maximum deviation of 0.5%. To reduce computing time in the following, we calculated P_S from crystal structure data based on one BEC tensor for each ion in the unit cell calculated for the GS only (given in Table I).

The results of the calculation of P_S according to Eq. (1) are shown in Fig. 4 for C-LN and S-LN (a) as well as for C-LT (b). P_S values based on DFT-relaxed structural parameters at given experimental unit-cell dimensions are shown in comparison (green). Additionally, we present P_S directly calculated with the Berry-phase expression in the same figure (blue). For further comparison, we added literature values of P_S for congruent and stoichiometric materials from experiments, as well as theoretical and semitheoretical values. The calculations of P_S directly from DFT or with the DFT-relaxed structure and BEC tensors show comparable results (see Fig. 4), but have a

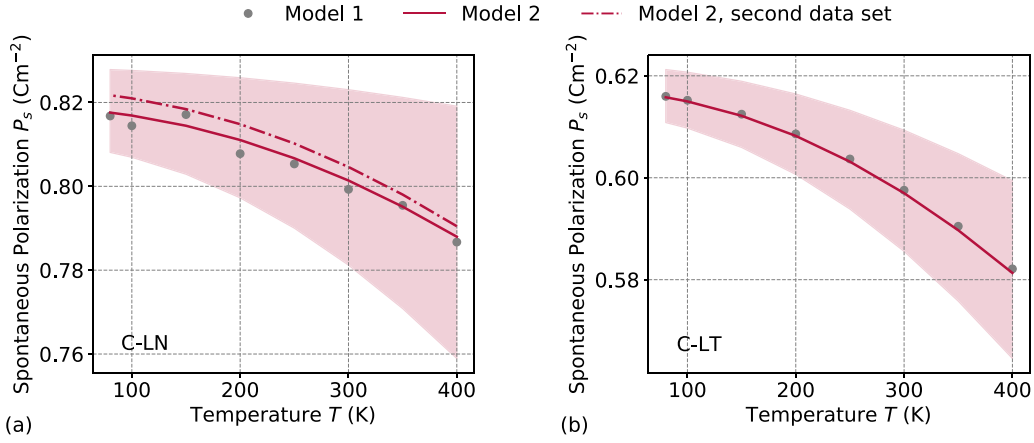


FIG. 3. Different models for the calculation of P_S for C-LN (a) and C-LT (b): Model 1 (gray dots) combined BEC tensors calculated for every temperature step with fitted structural parameters from SC-XRD (according to Fig. 1). Model 2 (red solid line) combined BEC tensors calculated exclusively for each ion in the unit cell at the GS with fitted structural parameters. For C-LN we measured a second data set (red dashed-dotted line) to show the reproducibility of the presented method. All values are within the 1σ confidence interval (light red areas).

high discrepancy with measured P_S values from literature and our results calculated with SC-XRD data. This is due to the underestimation of positional displacements from the center of charge with temperature, as discussed above. Therefore, we used only P_S calculated from SC-XRD structural data for the following determination of p .

C. Calculation of the pyroelectric coefficient

The results of p for congruent and stoichiometric materials, calculated with Eq. (2), are shown in Fig. 5 for LiNbO₃ (a) and for LiTaO₃ (b). Additionally, we measured p of the same crystals as used for preparation of the SC-XRD samples with the Sharp-Garn method for congruent and stoichiometric compositions. We added further values of p from literature for comparison. The values of P_S and p at $T = 300$ K are summarized in Table II.

IV. DISCUSSION

The computed P_S from the SC-XRD data corresponds perfectly with the results from Kitamura *et al.* [25] (see ■ in Fig. 4) for LiTaO₃ and for LiNbO₃ with the results from Gopalan *et al.* [24] (see ★ in Fig. 4). In comparison with other reported values, we rate the results from Gopalan *et al.* and Kitamura *et al.* as reliable since Gopalan *et al.* improved the

experimental setup with a capacitor in series with the sample to form an analog integration circuit. The capacitor voltage was read with a high-input impedance multimeter to avoid charge leakage. Otherwise, current spikes or the peak of the spikes will be missed [24], which results in lower P_S in the order of 0.70 C m^{-2} . Kitamura *et al.* used the same experimental setup as described by Gopalan *et al.* for the P_S measurements of LiTaO₃. Other experimental setups [21,93,94] determine significantly lower values for P_S . Measurements of P_S for LiNbO₃ and LiTaO₃ are challenging due to their high coercive fields and the elaborate sample preparation (thin polished samples with liquid electrodes are necessary) [21,24].

When we compare the accuracy of the calculated P_S and values from literature, the relative and absolute errors are in the same order of magnitude of $\approx 10\%$ and below 0.08 C m^{-2} , respectively. Slightly smaller errors occur for P_S computed with SC-XRD structure parameters (relative errors: C-LN 6%, S-LN 3%, C-LT 4%). However, the spread of the literature values (C-LN 0.3 C m^{-2} , S-LN 0.2 C m^{-2} , C-LT 0.1 C m^{-2}) is higher than the error for a single measured value and thus depends mainly on the experimental setup and sample preparation [21,24,93,94]. The error for the calculated P_S using SC-XRD data occurs mainly from errors of the crystal structure refinement and the resolution of the structural characterization method. More precise structure

TABLE I. BEC tensors of the GS at $T = 0$ K with positions Li = (x_1, y_1, z_1) , Nb/Ta = (x_1, y_1, z_1) , O = (x_1, y_1, z_1) for LiNbO₃ and LiTaO₃.

	LiNbO ₃			LiTaO ₃		
Li	1.128(5)	-0.122(9)	0	1.118(8)	-0.083(1)	0
	0.122(9)	1.128(5)	0	0.083(1)	1.118(8)	0
	0	0	1.023(2)	0	0	1.035(6)
Nb/Ta	7.058(9)	1.582(9)	0	6.641(2)	1.296(8)	0
	-1.582(9)	7.058(9)	0	-1.296(8)	6.641(3)	0
	0	0	7.603(9)	0	0	7.117(5)
O	-1.690(4)	0.091(6)	0.082(4)	-1.693(5)	0.059(2)	0.060(8)
	0.086(3)	-3.786(1)	-1.813(6)	0.042(8)	-3.479(9)	-1.595(8)
	0.126(9)	-1.868(6)	-2.875(7)	0.106(3)	-1.651(4)	-2.717(7)

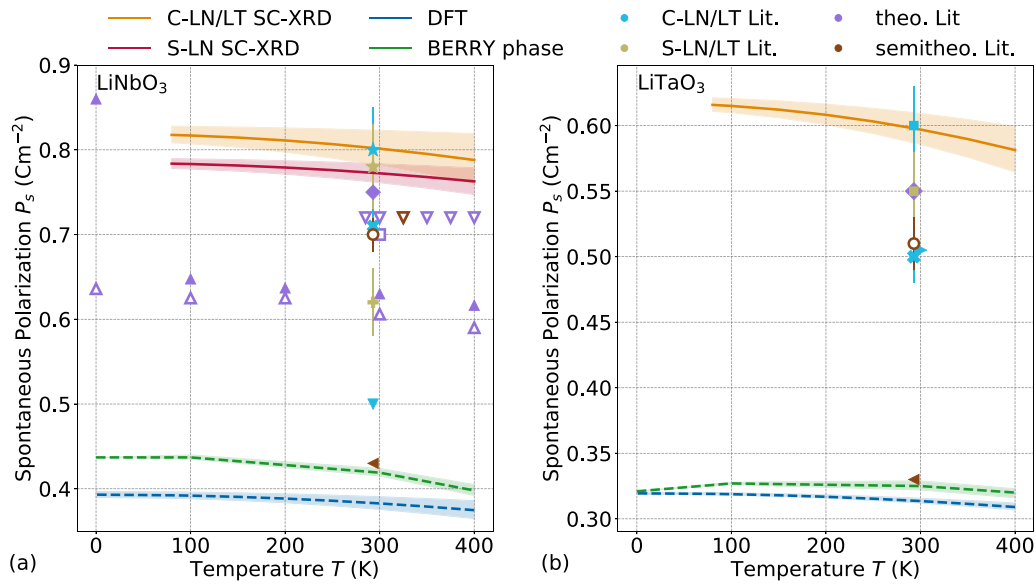


FIG. 4. Temperature-dependent spontaneous polarization of LiNbO_3 (a) as well as LiTaO_3 (b). The values are determined by different methods: calculated from SC-XRD determined crystal structures and computed BEC of the DFT-GS for congruent (C-LN/LT SC-XRD) and stoichiometric (S-LN SC-XRD) materials as well as DFT-relaxed atomic positions (DFT) and directly calculated with DFT (Berry phase). The light colored areas indicate the 1σ error range. Additional experimental literature values for congruent (C-LN/LT Lit.) and stoichiometric (S-LN/LT Lit.) material, as well as theoretical (theo. Lit) and semitheoretical (semitheo. Lit.) literature values are plotted with the following markers: \times [21], \star [24], $+$ [93], \blacksquare [25], ∇ [94], \blacklozenge [95], \blacktriangle [26], \blacktriangleleft [96], \blacktriangleright [97], \circ [98], \square [99], \triangle [100], ∇ [101].

parameters, e.g., determined by resonant diffraction methods [112,113] with specialized sample chamber equipment [114] or SC-XRD at synchrotron sources, would further improve the accuracy, but would also increase the experimental efforts.

In the literature, another approach to calculate P_S directly from the crystal structure can be found. Abrahams *et al.*

[98] used the displacement Δz of the p - or d -block metal ion with respect to P_S of five displacive ferroelectrics to determine P_S with a least-squares fit directly from Δz . However, this approach requires the knowledge of P_S and Δz of different materials to get a precise fit. Bergman *et al.* [100] used the deformation of the NbO_6 octahedron for the

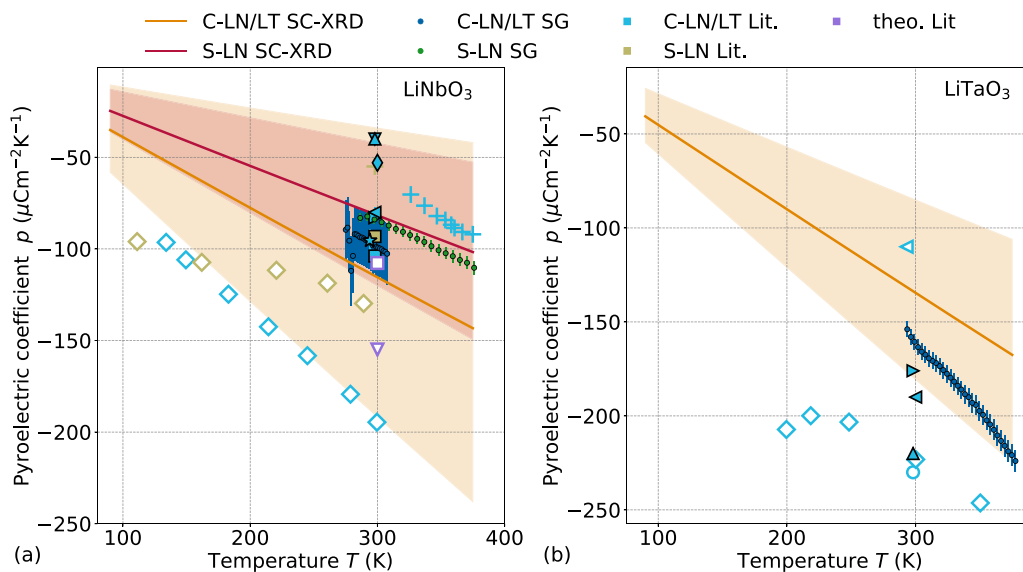


FIG. 5. The pyroelectric coefficient for LiNbO_3 (a) and LiTaO_3 (b) derived from P_S . Data calculated for experimental atomic positions from SC-XRD and BEC tensors for congruent (C-LN/LT SC-XRD) and stoichiometric (S-LN SC-XRD) material are shown. The light colored areas indicate the 1σ error range. Additionally, ρ was measured with the Sharp-Garn method for congruent (C-LN/LT SG) and stoichiometric (S-LN SG) LiNbO_3 as well as congruent LiTaO_3 crystals. Values from literature based on experiment for congruent (C-LN/LT Lit.) and stoichiometric (S-LN Lit.) as well as on theory (theo. Lit.) are shown for comparison: \star [102], \blacksquare [103], \blacklozenge [104], ∇ [94], $+$ [105], \blacktriangleleft [106], \blacktriangle [107], \blacktriangleright [108], \circ [109], \diamond [110], \square [26], ∇ [26], \blacktriangleleft [111].

TABLE II. Summary of the calculated P_S and p values for congruent (C) and stoichiometric (S) material using structural parameters determined from SC-XRD as well as measured p values using the Sharp-Garn method. Additionally, P_S for the DFT-relaxed structure calculated with BEC tensors (BEC) and with the Berry phase expression (Berry) as well as the resulting p are shown. P_S and p values from literature are listed for comparison. All values are given at $T = 300$ K. The 1σ error is shown in brackets.

	LiNbO ₃		LiTaO ₃	
	P_S (C m ⁻²)	p (μC m ⁻² K ⁻¹)	P_S (C m ⁻²)	p (μC m ⁻² K ⁻¹)
SC-XRD				
C	0.80(2)	-115(82)	0.60(2)	-134(49)
S	0.77(1)	-81(39)		
DFT				
BEC	0.382(8)	-79(33)	0.314(2)	-45(6)
Berry	0.419(5)	-150(15)	0.325(4)	-30(10)
Sharp-Garn				
C		-99(2)		-167(4)
S		-85(2)		-175(5)
Literature				
C	0.50 ... 0.80	-40 ... -194	0.50 ... 0.60	-110 ... -230
References	[21,24,94]	[94,102-108,110]	[21,25,97,109]	[97,107-111]
S	0.62 ... 0.78	-55 ... -93	0.55	
References	[24,93]	[103,110]	[25]	
Calculated	0.43 ... 0.75	-108 ... -155	0.33 ... 0.55	
References	[26,96,98-101]	[26]	[95,96,98]	

calculation of P_S , but they assumed the microscopic bond polarizability. Hsu *et al.* [96] used atomic displacements from synchrotron single-crystal x-ray diffraction and calculated Hirshfeld charges to obtain P_S , but the results show large deviations from the measured P_S since the experimentally determined charges (e.g., according to Hirshfeld or Bader) describe the charge inadequately and severely underestimate the dynamical redistribution of electron density in response to structural displacements [31]. The disadvantages of these approaches are eliminated in the presented work because we do not need the knowledge of further materials or material parameters and the charge distribution is correctly described by the BEC tensor.

The calculation of P_S with DFT leads to only one-half of the experimental values. The reason is, on the one hand, that the theory does not consider thermal ionic dynamics. The ions therefore do not test the full positional configuration range within the asymmetric local potential. Even using temperature-dependent unit-cell parameters from the experiment to improve the boundary conditions for the DFT calculations, the artificial external pressure can only approximate the overall internal pressure, but cannot capture its origin, which underestimates atomic displacements from the center of charge with temperature, as shown above. On the other hand, real structure influences like defects have not been considered, which may present further degrees of freedom for positional response and charge redistribution with temperature. Peng *et al.* [26] combine different approaches of molecular dynamic simulations to compute the temperature influence, which leads to higher computing time, but also to more realistic theoretical atomic displacements.

Thus, by computing BEC charges by means of DFT and measuring atomic displacements with high-resolution SC-XRD, our presented experimental-theoretical approach combines the best from the two worlds. Calculations using

experimentally determined structural parameters are more precise (see Fig. 4) than purely theoretical values and therefore recommended. Compared to conventional techniques, the semiempirical method provides the means for *in situ* monitoring of electric polarization changes within functional materials with assumed superior resolution in time (<1 μs) as well as space (<1 μm), which may pave the way towards designing new devices, e.g., based on standing acoustic waves [115-117].

The determined p with crystal structure data are in accordance (within the error range) with the experimental p and with reference values from the literature. Here, the calculated p for S-LN shows the highest agreement with the coefficients measured by the Sharp-Garn method with a maximum deviation of 10%. The coefficient for C-LN is found in the central mean of reference values from literature and deviates at most by 21%. For C-LT the coefficients determined by the Sharp-Garn method exceed our semitheoretical values at most by about 18%. The large variations of reported p values (C-LN: -40 μC m⁻² K⁻¹ ... -194 μC m⁻² K⁻¹, S-LN: -55 μC m⁻² K⁻¹ ... -93 μC m⁻² K⁻¹, C-LT: -110 μC m⁻² K⁻¹ ... -230 μC m⁻² K⁻¹) are mainly caused by the use of different measuring methods [94,97,105-109,118-121], which makes the determination of the correct value a very complex task [20]. Reported values of p can cover several orders of magnitude for the same material system [20]. In general, the maximum errors Δp of our calculated p values (C-LN ± 98 μC m⁻² K⁻¹, S-LN ± 48 μC m⁻² K⁻¹, C-LT ± 59 μC m⁻² K⁻¹) are significantly larger than for the experimentally determined values using the Sharp-Garn method (C-LN ± 20 μC m⁻² K⁻¹, S-LN ± 5 μC m⁻² K⁻¹, C-LT ± 6 μC m⁻² K⁻¹), but are in the range of the spread of p measured with various other methods. Again, a strong dependence on the experimental setup is apparent. The method presented here is a static

method [20] for the determination of p . A further approach to get access to the pyroelectric coefficient was presented by Madsen *et al.* [122]. They showed that the pyroelectric coefficient of molecular organic crystal structures can be determined from experimental structure data for organic molecules using a multipolar modeling of x-ray diffraction data with relative errors of 18%. However, this approach gives only access to p and not to P_s .

The primary pyroelectric coefficient results from the movement of cations relative to anions without any change in the unit-cell dimensions. However, these dimensions change due to thermal expansion, resulting in mechanical stress. As all pyroelectric materials are also piezoelectric, this will contribute to the pyroelectric effect [121], which is reflected in the secondary pyroelectric coefficient. For an unclamped sample (free expansion, constant stress), as in this work, the determined p is the sum of the primary and secondary effects [see Eq. (3)] and the contributions cannot be separated. The secondary pyroelectric coefficient can be evaluated according to

$$p_{k,sec} = d_{klm}^{T,E} C_{lmij}^{T,E} \alpha_{ij}^{\sigma,E} \quad (4)$$

with the thermal expansion coefficient $\alpha_{ij}^{\sigma,E}$ (at constant electric field E and strain σ), the elastic stiffness tensor $C_{lmij}^{T,E}$ (at constant T and E), and the piezoelectric stress coefficient $d_{klm}^{T,E}$ (at constant T and E). $\alpha_{ij}^{\sigma,E}$ can be easily determined from temperature-dependent structural data (see Appendix A). $C_{lmij}^{T,E}$ and $d_{klm}^{T,E}$ can be measured experimentally or calculated by density functional perturbation theory (DFPT), as shown, e.g., by Peng *et al.* [26]. We have calculated p_{sec} (considering only contributions parallel to \vec{c}) according to Eq. (4) with $\alpha_{ij}^{\sigma,E}$ from Table IV and with $C_{lmij}^{T,E}$ and $d_{klm}^{T,E}$ from Smith and Welsh [123] for C-LN and C-LT. The results are presented in Table III and are comparable with the results of Peng [26] and in the same order of magnitude as the literature values [121].

Since our measurements were performed under constant stress of the material (free expansion), all coefficients of the piezoelectric tensor are coupled and cannot be directly determined from the experimental data. For a calculation of $d_{klm}^{T,E}$ from crystal structure data further constraints, like fixed in-plane lattice parameters to evaluate the out-of-plane piezoelectric coefficient, need to be considered.

The determination of P_s and p directly from crystal structure data has considerable advantages. On the one hand, the approach is not prone to any spurious contribution in the electric measurement of the pyroelectric current, like dis-

turbing contributions from the experimental setup or trapped states inducing thermally stimulated currents. This becomes particularly important for conductive samples or samples with thermally induced conductivity. On the other hand, the presented approach proves to be more reliable than conventional *ab initio* calculations, where the necessary modeling of thermal motions of the atoms is still challenging. As a welcome benefit, by employing the temperature-dependent structural characterization, the method gives direct access to the structural origin of the polar properties as well as the quantitative contributions from specific changes in the crystal structure.

V. CONCLUSION

In this work, we demonstrate the direct calculation of the spontaneous polarization and pyroelectric coefficient of a material, as proposed by Peng *et al.* [26], from experimental temperature-dependent crystal structure data. With smoothed structure parameters to reduce experimental fluctuations (e.g., induced by environmental parameter variations [124]) and one set of BEC tensors computed by DFT at $T = 0$ K, reliable and reproducible results were obtained. By limiting BEC computation to the GS, which significantly reduces the computational cost of the method, the introduced errors in spontaneous polarization are $\leq 1\%$. The calculated polarization based on temperature-dependent SC-XRD refinements is in good agreement with reference values from literature.

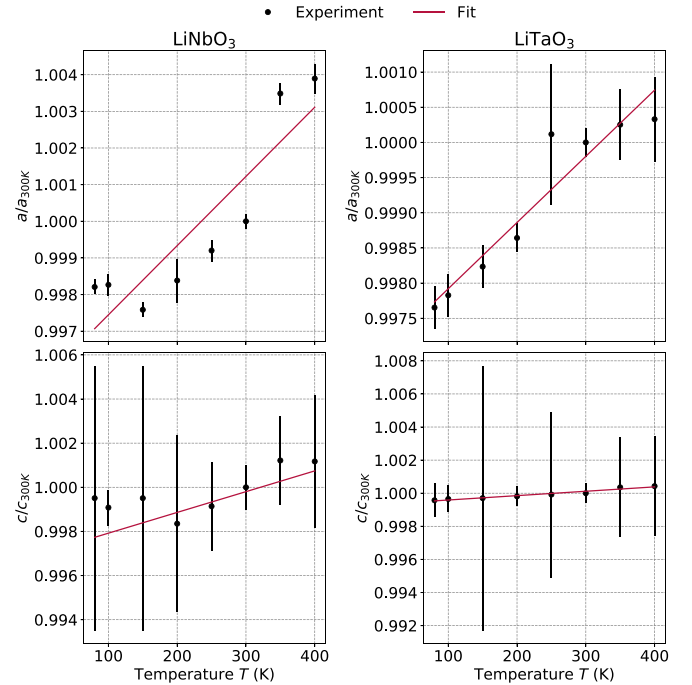


FIG. 6. Fit of the thermal expansion coefficients α_a along the crystallographic axis a and α_c along axis c for congruent LiNbO_3 (left) and LiTaO_3 (right). The temperature-dependent lattice parameters are normalized to the lattice parameters at $T = 300$ K. The thermal expansion coefficients were determined with a linear fit, which resembles well the dependence in the range between 100 and 400 K.

TABLE III. Results of p_{sec} according to Eq. (4) using the experimentally determined $\alpha_{ij}^{\sigma,E}$ together with $C_{lmij}^{T,E}$ and $d_{klm}^{T,E}$ from Ref. [123]. The obtained values (SC-XRD) are compared with experimental (Expt.) [121] and calculated (Calc.) [26] values from literature.

	C-LN	C-LT
SC-XRD p_{sec} ($\mu\text{C m}^{-2} \text{K}^{-1}$)	16.6(4)	-3.6(4)
Expt. p_{sec} ($\mu\text{C m}^{-2} \text{K}^{-1}$)	12.8	-1
Calc. p_{sec} ($\mu\text{C m}^{-2} \text{K}^{-1}$)	17.0	

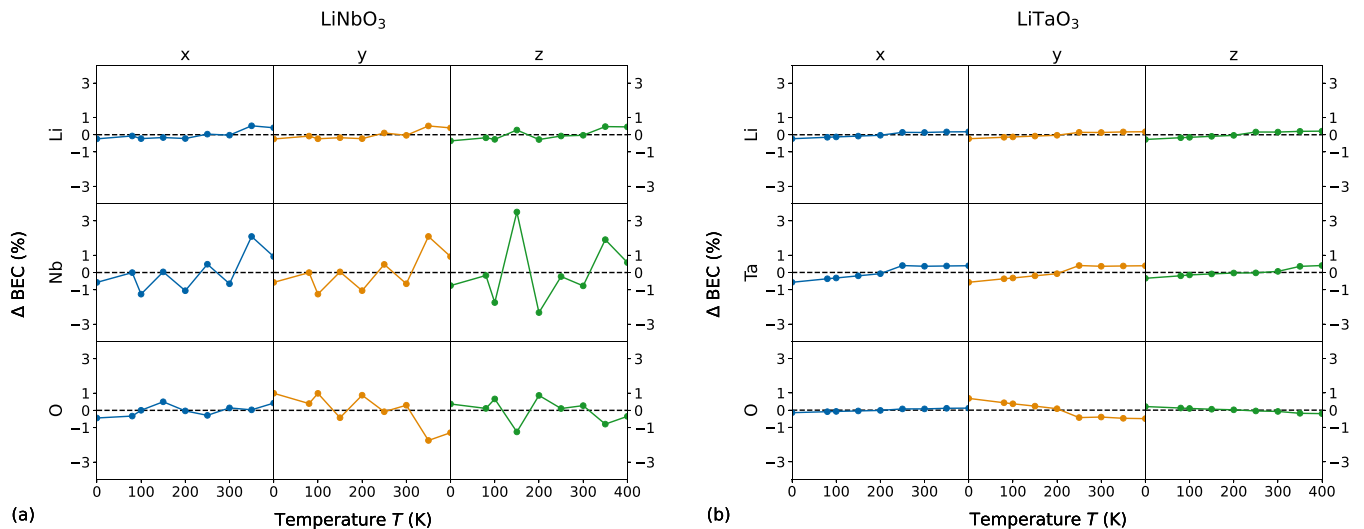


FIG. 7. BEC data for both systems LiNbO_3 (a) and LiTaO_3 (b) using the experimentally (with SC-XRD) determined lattice parameters for the temperatures above 0 K and extrapolated lattice parameters at 0 K.

The combined experimental-theoretical approach is superior to exclusive *ab initio* DFT models, which predict significantly smaller polarization values due to smaller displacements from the center of charge.

The present results are based on experimental data acquired with a standard laboratory diffractometer, which at present induces the largest uncertainties in the calculations. However, the approach is easy to apply because only temperature-dependent structural data and a BEC tensor are needed. There is no need for an additional experimental setup to carry out electrical measurements. Additionally, to gain an understanding of the underlying physical effects, the comprehensive structural data show the structural origin of the polar properties and correlate directly changes in the crystal structure characteristics (defect structure, atomic displacements) with changes in the polarization.

Methodical accuracy from these first examples using experimental structure determination can be assessed as remarkable, as the results for the calculation of the pyroelectric coefficients fit well into the spread of reported literature values, and they also overlap with experimental results using the highly reliable Sharp-Garn method [20]. This makes the presented method a well-recommended alternative for the determination of polarization and pyroelectric coefficients, where conventional electrical methods are difficult or not feasible at all, e.g., due to sample size and preparation requirements, sample conductivity, or other experimental obstacles. SC-XRD data from modern structure determination methods, e.g., using resonant x-ray diffraction techniques, would further improve the methodical validity.

ACKNOWLEDGMENTS

The authors would like to thank U. Fischer for sample preparation as well as Dr. M. Kaiser (TU Dresden) and Prof. Dr. A. Lubk (IFW Dresden) for experimental and theoretical support. For financial support, the Deutsche Forschungsgemeinschaft (DFG Grants No. 409743569 and

No. 324641898), the Federal Ministry of Education and Research (Grant No. 0325563A), the free state of Saxony (Grant No. INST26786-1FUGG), the European Regional Development Fund, and the Ministry of Science and Art of Saxony (Grant No. 100109976) are gratefully acknowledged. Furthermore, we acknowledge the Compute Cluster 2019 of the Faculty of Mathematics and Computer Science of Technische Universität Bergakademie Freiberg, operated by the computing center (URZ) and funded by the DFG (Grant No. 397252409) for provision of high-performance computing for BEC and DFT calculations.

APPENDIX A: CALCULATION OF THE THERMAL EXPANSION COEFFICIENTS

According to Kim *et al.* [75], the thermal expansion coefficients can be calculated by fitting the temperature-dependent lattice parameters normalized to the lattice parameters at $T = 300$ K (see Fig. 6). For direct access to the linear expansion coefficient of our crystals, we fitted the data linearly. The results are given in Table IV.

APPENDIX B: TEMPERATURE DEPENDENCY OF BEC TENSORS

The calculated BEC data for all temperatures based on the experimentally determined lattice parameters are shown

TABLE IV. Linear thermal expansion coefficients α from the fit (see Fig. 6) of experimentally (Expt.) determined lattice parameters a and c for congruent material, as well as reference (Lit.) values from Kim *et al.* [75].

	α_a (10^{-6} K^{-1})		α_c (10^{-6} K^{-1})	
	Expt.	Lit.	Expt.	Lit.
LiNbO_3	18.9(4)	15.4	6.5(2)	7.5
LiTaO_3	9.0(1)	16.2	2.6(3)	2.2

in Fig. 7. Since the BEC tensors were calculated with the experimental lattice parameters, they show fluctuations as well. However, the errors in the BEC tensors are only in the

order of a few percent and are negligible in comparison to the experimental displacement errors for the calculation of the spontaneous polarization.

-
- [1] D. Zhang, H. Wu, C. R. Bowen, and Y. Yang, *Small* **17**, 2103960 (2021).
- [2] M. H. Lee, R. Guo, and A. S. Bhalla, *J. Electroceram.* **2**, 229 (1998).
- [3] R. Whatmore, *Rep. Prog. Phys.* **49**, 1335 (1986).
- [4] Y. Yang, Y. Zhou, J. M. Wu, and Z. L. Wang, *ACS Nano* **6**, 8456 (2012).
- [5] X. Wang, Y. Dai, R. Liu, X. He, S. Li, and Z. L. Wang, *ACS Nano* **11**, 8339 (2017).
- [6] U. Sassi, R. Parret, S. Nanot, M. Bruna, S. Borini, D. De Fazio, Z. Zhao, E. Lidorikis, F. H. L. Koppens, and A. C. Ferrari, *Nat. Commun.* **8**, 1 (2017).
- [7] G. Rosenman, D. Shur, Y. E. Krasik, and A. Dunaevsky, *J. Appl. Phys.* **88**, 6109 (2000).
- [8] E. Gutmann, A. Benke, K. Gerth, H. Böttcher, E. Mehner, C. Klein, U. Krause-Buchholz, U. Bergmann, W. Pompe, and D. C. Meyer, *J. Phys. Chem. C* **116**, 5383 (2012).
- [9] M. Sharma, G. Singh, and R. Vaish, *J. Am. Ceram. Soc.* **103**, 4774 (2020).
- [10] A. Kakekhani and S. Ismail-Beigi, *J. Mater. Chem. A* **4**, 5235 (2016).
- [11] Y. Inoue, *Energy Environ. Sci.* **2**, 364 (2009).
- [12] B. Zielińska, E. Borowiak-Palen, and R. J. Kalenzuk, *J. Phys. Chem. Solids* **69**, 236 (2008).
- [13] M. Zhang, Q. Hu, K. Ma, Y. Ding, and C. Li, *Nano Energy* **73**, 104810 (2020).
- [14] D. Navid, A. and Vanderpool, A. Bah, and L. Pilon, *Int. J. Heat Mass Transf.* **53**, 4060 (2010).
- [15] R. B. Olsen, D. A. Bruno, and J. M. Briscoe, *J. Appl. Phys.* **58**, 4709 (1985).
- [16] H. Nguyen, A. Navid, and L. Pilon, *Appl. Therm. Eng.* **30**, 2127 (2010).
- [17] A. Sultana, M. M. Alam, T. R. Middy, and D. Mandal, *Appl. Energy* **221**, 299 (2018).
- [18] M. U. de Vivanco, M. Zschornak, H. Stöcker, S. Jachalke, E. Mehner, T. Leisegang, and D. C. Meyer, *Phys. Chem. Chem. Phys.* **22**, 17781 (2020).
- [19] I. Lubomirsky and O. Stafsudd, *Rev. Sci. Instrum.* **83**, 051101 (2012).
- [20] S. Jachalke, E. Mehner, H. Stöcker, J. Hanzig, M. Sonntag, T. Weigel, T. Leisegang, and D. C. Meyer, *Appl. Phys. Rev.* **4**, 021303 (2017).
- [21] S. H. Wemple, M. DiDomenico, and I. Camlibel, *Appl. Phys. Lett.* **12**, 209 (1968).
- [22] K. Miyasato, S. Abe, H. Takezoe, A. Fukuda, and E. Kuze, *Jpn. J. Appl. Phys.* **22**, L661 (1983).
- [23] D. Lebeugle, D. Colson, A. Forget, and M. Viret, *Appl. Phys. Lett.* **91**, 022907 (2007).
- [24] V. Gopalan, T. E. Mitchell, Y. Furukawa, and K. Kitamura, *Appl. Phys. Lett.* **72**, 1981 (1998).
- [25] K. Kitamura, Y. Furukawa, K. Niwa, V. Gopalan, and T. E. Mitchell, *Appl. Phys. Lett.* **73**, 3073 (1998).
- [26] Q. Peng and R. E. Cohen, *Phys. Rev. B* **83**, 220103(R) (2011).
- [27] V. Srinivasan, R. Gebauer, R. Resta, and R. Car, *AIP Conference Proceedings* **677**, 168 (2003).
- [28] K. M. Rabe, C. H. Ahn, and J. M. Triscone, *Physics of Ferroelectrics: A Modern Perspective*, Topics in Applied Physics (Springer, Berlin, 2007).
- [29] H.-C. Thong, X. Y. Wang, J. Han, L. Zhang, B. Li, K. Wang, and B. Xu, *Phys. Rev. B* **107**, 014101 (2023).
- [30] J. Ghosez and P. Junquera, *Annu. Rev. Condens. Matter Phys.* **13**, 325 (2022).
- [31] R. Resta and D. Vanderbilt, *Physics of Ferroelectrics* (Springer, Berlin, 2007), pp. 31–68.
- [32] R. Clausius, *Die Mechanische Behandlung der Electrica* (Vieweg, Berlin, 1879).
- [33] O. F. Mossotti, *Memorie di Matematica e di Fisica della Società Italiana delle Scienze Residente in Modena* **24**, 49 (1850).
- [34] R. Resta, *Rev. Mod. Phys.* **66**, 899 (1994).
- [35] R. D. King-Smith and D. Vanderbilt, *Phys. Rev. B* **47**, 1651 (1993).
- [36] D. Vanderbilt and R. D. King-Smith, *Phys. Rev. B* **48**, 4442 (1993).
- [37] M. Veithen and P. Ghosez, *Phys. Rev. B* **65**, 214302 (2002).
- [38] W. Zhong, R. D. King-Smith, and D. Vanderbilt, *Phys. Rev. Lett.* **72**, 3618 (1994).
- [39] L. Hafid and F. M. Michel-Calendini, *J. Phys. C: Solid State Phys.* **19**, 2907 (1986).
- [40] J. B. Neaton, C. Ederer, U. V. Waghmare, N. A. Spaldin, and K. M. Rabe, *Phys. Rev. B* **71**, 014113 (2005).
- [41] F. Bernardini, V. Fiorentini, and D. Vanderbilt, *Phys. Rev. B* **56**, R10024 (1997).
- [42] A. Roy, S. Mukherjee, R. Gupta, S. Auluck, R. Prasad, and A. Garg, *J. Phys.: Condens. Matter* **23**, 325902 (2011).
- [43] A. Roy, R. Prasad, S. Auluck, and A. Garg, *J. Phys.: Condens. Matter* **22**, 165902 (2010).
- [44] C. Z. Wang, R. Yu, and H. Krakauer, *Phys. Rev. B* **54**, 11161 (1996).
- [45] D. D. Fong, C. Cionca, Y. Yacoby, G. B. Stephenson, J. A. Eastman, P. H. Fuoss, S. K. Streiffer, C. Thompson, R. Clarke, R. Pindak, and E. A. Stern, *Phys. Rev. B* **71**, 144112 (2005).
- [46] G. Donnay, *Acta Crystallogr., Sect. A* **33**, 927 (1977).
- [47] R. S. Weis and T. K. Gaylord, *Appl. Phys. A* **37**, 191 (1985).
- [48] M. E. Lines and A. M. Glass, *Principles and Applications of Ferroelectrics and Related Materials*, reprinted. ed. (Clarendon, Oxford, 2009).
- [49] S. C. Abrahams, H. J. Levinstein, and J. M. Reddy, *J. Phys. Chem. Solids* **27**, 1019 (1966).
- [50] S. C. Abrahams and J. L. Bernstein, *J. Phys. Chem. Solids* **28**, 1685 (1967).
- [51] S. C. Abrahams, J. M. Reddy, and J. L. Bernstein, *J. Phys. Chem. Solids* **27**, 997 (1966).
- [52] T. Köhler, E. Mehner, J. Hanzig, G. Gärtner, C. Funke, Y. Joseph, T. Leisegang, H. Stöcker, and D. C. Meyer, *J. Mater. Chem. C* **9**, 2350 (2021).

- [53] T. Köhler, M. Zschornak, C. Röder, J. Hanzig, G. Gärtner, T. Leisegang, E. Mehner, H. Stöcker, and D. C. Meyer, *J. Mater. Chem. C* **11**, 520 (2023).
- [54] T. Köhler, E. Mehner, J. Hanzig, G. Gärtner, H. Stöcker, T. Leisegang, and D. C. Meyer, *J. Solid State Chem.* **244**, 108 (2016).
- [55] M. Nentwich, M. Zschornak, T. Weigel, T. Köhler, D. Novikov, D. C. Meyer, and C. Richter (unpublished).
- [56] L. E. Garn and E. J. Sharp, *J. Appl. Phys.* **53**, 8974 (1982).
- [57] E. J. Sharp and L. E. Garn, *J. Appl. Phys.* **53**, 8980 (1982).
- [58] T. Weigel, C. Funke, M. Zschornak, T. Behm, H. Stöcker, T. Leisegang, and D. C. Meyer, *J. Appl. Crystallogr.* **53**, 614 (2020).
- [59] Bruker AXS Inc., *DOC-M86-EXX190 D8 QUEST User Manual* (Madison, Wisconsin, US, 2012).
- [60] Bruker AXS Inc., *DOC-M86-EXX229 APEX3 Software User Manual* (Madison, Wisconsin, US, 2016).
- [61] V. Petříček, M. Dusek, and L. Palatinus, *Z. Kristallogr.* **229**, 345 (2014).
- [62] G. Kresse and J. Furthmüller, *Phys. Rev. B* **54**, 11169 (1996).
- [63] G. Kresse and D. Joubert, *Phys. Rev. B* **59**, 1758 (1999).
- [64] J. P. Perdew, K. Burke, and M. Ernzerhof, *Phys. Rev. Lett.* **77**, 3865 (1996).
- [65] H. J. Monkhorst and J. D. Pack, *Phys. Rev. B* **13**, 5188 (1976).
- [66] E. Mehner, S. Jachalke, J. Hanzig, T. Leisegang, H. Stöcker, and D. C. Meyer, *Ferroelectrics* **510**, 132 (2017).
- [67] S. Jachalke, T. Schenk, M. H. Park, U. Schroeder, T. Mikolajick, H. Stöcker, E. Mehner, and D. C. Meyer, *Appl. Phys. Lett.* **112**, 142901 (2018).
- [68] T. Hahn, *International Tables for Crystallography*, 5th ed. (Kluwer Academic, Dordrecht, 2002).
- [69] P. Paufler, *Physikalische Kristallographie* (Wiley-VCH, Weinheim, 1986).
- [70] I. Inbar and R. E. Cohen, *Phys. Rev. B* **53**, 1193 (1996).
- [71] I. Inbar and R. E. Cohen, *Ferroelectrics* **194**, 83 (1997).
- [72] S. B. Lang, *Sourcebook of Pyroelectricity* (Gordon and Breach, New York, 1974).
- [73] See Supplemental Material at <http://link.aps.org/supplemental/10.1103/PhysRevB.108.054105> for cif files from single-crystal x-ray diffraction refinements.
- [74] I. A. Guzei, G. A. Bikzhanova, L. C. Spencer, T. V. Timofeeva, T. L. Kinnibrugh, and C. F. Campana, *Cryst. Growth Des.* **8**, 2411 (2008).
- [75] Y. S. Kim and R. T. Smith, *J. Appl. Phys.* **40**, 4637 (1969).
- [76] C. Kittel, J. M. Gress, and A. Lessard, *Einführung in die Festkörperphysik*, 12th ed. (Oldenbourg, München, 1999).
- [77] S. Srivastava and V. I. Shamanin, *SOPTrans. Appl. Chem.* **1**, 1 (2014).
- [78] L. He, F. Liu, G. Hautier, M. J. T. Oliveira, M. A. L. Marques, F. D. Vila, J. J. Rehr, G.-M. Rignanese, and A. Zhou, *Phys. Rev. B* **89**, 064305 (2014).
- [79] N. Zotov, H. Boysen, F. Frey, T. Metzger, and E. Born, *J. Phys. Chem. Solids* **55**, 145 (1994).
- [80] S. C. Abrahams and P. Marsh, *Acta Crystallogr., Sect. B: Struct. Sci.* **42**, 61 (1986).
- [81] A. Vyalikh, M. Zschornak, T. Köhler, M. Nentwich, T. Weigel, J. Hanzig, R. Zaripov, E. Vavilova, S. Gemming, E. Brendler, and D. C. Meyer, *Phys. Rev. Mater.* **2**, 013804 (2018).
- [82] K. Momma and F. Izumi, *J. Appl. Crystallogr.* **44**, 1272 (2011).
- [83] M. Volk and T. Wöhlecke, *Lithium Niobate: Defects, Photorefractive and Ferroelectric Switching*, Springer Series in Materials Science, Vol. 115 (Springer, Berlin, 2008).
- [84] H. Hatano, K. Kitamura, and Y. Liu, in *Photorefractive Materials and Their Applications 2* (Springer, Berlin, 2007), pp. 127–164.
- [85] T. Köhler, M. Zschornak, M. Zbiri, J. Hanzig, C. Röder, C. Funke, H. Stöcker, E. Mehner, and D. C. Meyer, *J. Mater. Chem. C* **9**, 13484 (2021).
- [86] S. Miyazawa and H. Iwasaki, *J. Cryst. Growth* **10**, 276 (1971).
- [87] K. Chen, Y. Li, C. Peng, Z. Lu, X. Luo, and D. Xue, *Inorg. Chem. Front.* **8**, 4006 (2021).
- [88] J. Rahn, E. Hüger, L. Dörrer, B. Ruprecht, P. Heitjans, and H. Schmidt, *Phys. Chem. Chem. Phys.* **14**, 2427 (2012).
- [89] N. Zotov, F. Frey, H. Boysen, H. Lehnert, A. Hornsteiner, B. Strauss, R. Sonntag, H. M. Mayer, F. Güthoff, and D. Hohlwein, *Acta Crystallogr., Sect. B: Struct. Sci.* **51**, 961 (1995).
- [90] N. Iyi, K. Kitamura, F. Izumi, J. K. Yamamoto, T. Hayashi, H. Asano, and S. Kimura, *J. Solid State Chem.* **101**, 340 (1992).
- [91] H. Boysen and F. Altorfer, *Acta Crystallogr., Sect. B: Struct. Sci.* **50**, 405 (1994).
- [92] S. C. Abrahams, E. Buehler, W. C. Hamilton, and S. J. Laplaca, *J. Phys. Chem. Solids* **34**, 521 (1973).
- [93] Y. Chen, J. Xu, X. Chen, Y. Kong, and G. Zhang, *Opt. Commun.* **188**, 359 (2001).
- [94] A. Savage, *J. Appl. Phys.* **37**, 3071 (1966).
- [95] S. Kim, V. Gopalan, and A. Gruverman, *Appl. Phys. Lett.* **80**, 2740 (2002).
- [96] R. Hsu, E. N. Maslen, D. Du Boulay, and N. Ishizawa, *Acta Crystallogr., Sect. B: Struct. Sci.* **53**, 420 (1997).
- [97] M. Kovář, L. Dvořák, and S. Černý, *Appl. Surf. Sci.* **74**, 51 (1994).
- [98] S. C. Abrahams, S. K. Kurtz, and P. B. Jamieson, *Phys. Rev.* **172**, 551 (1968).
- [99] R. I. Shostak, S. V. Yevdokimov, and A. V. Yatsenko, *Crystallogr. Rep.* **54**, 492 (2009).
- [100] J. G. Bergman, *Chem. Phys. Lett.* **38**, 230 (1976).
- [101] S. R. Phillpot and V. Gopalan, *Appl. Phys. Lett.* **84**, 1916 (2004).
- [102] S. T. Popescu, A. Petris, and V. I. Vlad, *J. Appl. Phys.* **113**, 043101 (2013).
- [103] J. Parravicini, J. Safioui, V. Degiorgio, P. Minzioni, and M. Chauvet, *J. Appl. Phys.* **109**, 033106 (2011).
- [104] S. V. Yevdokimov, R. I. Shostak, and A. V. Yatsenko, *Phys. Solid State* **49**, 1957 (2007).
- [105] T. Bartholomäus, K. Buse, C. Deuper, and E. Krätzig, *Phys. Status Solidi A* **142**, K55 (1994).
- [106] B. C. Grabmaier, W. Wersing, and W. Koestler, *J. Cryst. Growth* **110**, 339 (1991).
- [107] H. P. Beerman, *Infrared Phys.* **15**, 225 (1975).
- [108] S. B. Lang, *Phys. Today* **58**(8), 31 (2005).
- [109] M. Kao, M. Lee, C. Wang, H. Chen, and Y. Chen, *Jpn. J. Appl. Phys.* **41**, 2982 (2002).
- [110] A. M. Glass and M. Lines, *Phys. Rev. B* **13**, 180 (1976).
- [111] S.-L. Young, M.-C. Kao, and H.-Z. Chen, *J. Electroceram.* **17**, 799 (2006).
- [112] M. Zschornak, C. Richter, M. Nentwich, H. Stöcker, S. Gemming, and D. C. Meyer, *Cryst. Res. Technol.* **49**, 43 (2014).

- [113] C. Richter, M. Zschornak, D. Novikov, E. Mehner, M. Nentwich, J. Hanzig, S. Gorfman, and D. C. Meyer, *Nat. Commun.* **9**, 1 (2018).
- [114] M. Nentwich, T. Weigel, C. Richter, H. Stöcker, E. Mehner, S. Jachalke, D. V. Novikov, M. Zschornak, and D. C. Meyer, *J. Synchrotron Radiat.* **28**, 158 (2021).
- [115] Y. A. Eliovich, E. N. Ovchinnikova, K. A. Kozlovskaya, M. Zschornak, T. Weigel, C. Ludt, A. E. Blagov, V. E. Dmitrienko, Y. V. Pisarevskii, and M. V. Koval'chuk, *JETP Lett.* **115**, 456 (2022).
- [116] H. Stöcker, J. Hanzig, M. Zschornak, E. Mehner, S. Jachalke, C. Richter, F. Hanzig, F. Meutzner, T. Leisegang, and D. C. Meyer, *Cryst. Res. Technol.* **52**, 1600222 (2017).
- [117] M. Zschornak, J. Hanzig, H. Stöcker, T. Leisegang, S. Gemming, and D. C. Meyer, in *Switching Effects in Transition Metal Oxides*, edited by K. Roleder, W. Speier, and K. Szot (Wydawnictwo Naukowe PWN, Warszawa, 2021).
- [118] J. C. Joshi and A. L. Dawar, *Phys. Status Solidi A* **70**, 353 (1982).
- [119] J. S. Kim, J. B. Kim, B. C. Choi, C. S. Kim, J. H. Ro, and J. N. Kim, *J. Korean Phys. Soc.* **24**, 343 (1991).
- [120] P. W. Haycock and P. D. Townsend, *Appl. Phys. Lett.* **48**, 698 (1986).
- [121] R. E. Newnham, *Properties of Materials: Anisotropy, Symmetry, Structure* (Oxford University Press, Oxford, 2005).
- [122] G. K. H. Madsen, F. C. Krebs, B. Lebech, and F. K. Larsen, *Chem. Eur. J.* **6**, 1797 (2000).
- [123] R. T. Smith and F. S. Welsh, *J. Appl. Phys.* **42**, 2219 (1971).
- [124] T. Weigel, T. Leisegang, M. Zschornak, M. Herrmann, M. Rothenberger, A. Wünsche, H. Stöcker, and D. C. Meyer, *J. Appl. Crystallogr.* **48**, 1870 (2015).